Electronic Supplementary Material (ESI) for Journal of Materials Chemistry A.

Supporting Information

Structural and defect modulations of co-precipitation synthesized high-entropy Prussian blue analogue nanocubes via Cu/Zn co-doping for enhanced electrochemical performance

Van Thanh Nguyen[#], Fitri Nur Indah Sari[#], Brahmanu Wisnu Saputro, Jyh-Ming Ting[*]

Department of Materials Science and Engineering

University, No 1 University Road, Tainan 70101, Taiwan

[*] Corresponding author: jting@mail.ncku.edu.tw

[#] Equal contribution 1st author

Information S1

The ion diffusion coefficient is estimated using the Randles-Sevick equation:

$$I_p = (2.69 \times 10^5)\, n^{1.5} A D^{0.5} C \nu^{0.5} \quad \text{(S1)}$$

where Ip is the peak current, n is the number of electrons transferred, A is the surface area of the electrode, D is ion diffusion coefficient, C is the ion concentration in the electrolyte, and ν is the scan rate. In general, n, A, and C are constants. Thus, the slope of the plot of Ip vs. $\nu^{0.5}$ represents the ion diffusion rate.

Information S2

The percentages of surface capacitive and diffusion-controlled charge storages are estimated using Equation S2.

$$i(V) = k_1 \nu + k_2 \nu^{1/2} \quad \text{(S2)}$$

where i(V) is the current at a constant potential, k_1 and k_2 are the constants, and v is the scan rate. $k_1\nu$ and $k_2\nu^{1/2}$ represent the surface-capacitive and diffusion-controlled current, respectively. From Equation S2, by plotting $i(V)/\nu^{1/2}$ vs $\nu^{1/2}$, the values of k_1 and k_2 can be determined from the slope and the intercept of the curve, respectively. From the k_1 and k_2 values at specific potential, the percentage of the currents from surface-capacitive and diffusion-controlled can be calculated.

Table S1. ICP and EA concentrations of the obtained samples.

Sample ID	ICP (wt%)						EA (wt%)			ΔS_{conf}
	Fe	Co	Ni	Mn	Cu	Zn	C	N	H	
CNM	47.5	21.1	8.5	22.9	0.0	0.0	19.4	22.3	1.27	1.22 R
CNMCu	44.8	13.2	5.2	13.9	22.9	0.0	18.4	21	1.58	1.38R
CNMZn	41.9	12.1	7.2	13.5	0.0	25.3	18.7	21.3	1.55	1.42R
CNMCuZn	43.1	10.7	5.9	9.8	14.0	16.5	18.6	21	1.58	1.55R
CNM2CuZn	40.4	8.8	8.6	8.0	19.5	14.7	17.6	19.8	2.06	1.57R
CNMCu2Zn	40.1	6.1	5.0	6.3	16.8	25.9	16.7	18.4	2.41	1.51R
CNM2Cu2Zn	35.7	6.1	4.1	4.7	20.6	28.8	17.9	20	2.03	1.51R

The configurational entropy (ΔS_{conf}) of an n component system can be calculated using below equation[1, 2]:

$$\Delta S_{conf} = -R\sum_{i=1}^{n} x_i \ln x_i \qquad \text{(S3)}$$

where R is the ideal gas constant and x_i is the molar fraction of the i^{th} component.

Table S2. Average particle sizes of as-prepared PBAs.

Sample ID	Average particle size (nm)
CNM	292 ± 34
CNMCu	307 ± 46
CNMZn	226 ± 19
CNMCuZn	158 ± 25
CNM2CuZn	170 ± 38
CNMCu2Zn	128 ± 33
CNM2Cu2Zn	130 ± 21

Table S3. BET surface area, and pore size and volume.

Sample ID	BET surface area (m^2 g^{-1})	Pore size (nm)	Pore volume (cm^2 g^{-1})
CNM	6.2	10.9	0.017
CNMCu	8.9	12.8	0.029
CNMZn	24.8	26.6	0.153
CNMCuZn	167.1	3.2	0.134
CNM2CuZn	385.8	2.7	0.256
CNMCu2Zn	596.9	2.9	0.439
CNM2Cu2Zn	539.8	3.0	0.383

Table S4. The x, y and z values in $K_xM[Fe(CN)_6]_y[\square Fe(CN)_6]_{(1-y)}.zH_2O$.

Sample ID	x	y	Z
CNM	1.58	0.93	2.37
CNMCu	1.28	0.87	4.04
CNMZn	0.96	0.78	3.25
CNMCuZn	0.98	0.83	5.19
CNM2CuZn	0.93	0.74	4.34
CNMCu2Zn	0.76	0.77	3.33
CNM2Cu2Zn	0.38	0.62	4.11

Table S5. Comparison of electrochemical performances of PBA-based materials.

Materials	Capacitance (capacity)	Cycle stability	Electrolyte	Refs
CNM2Cu2Zn HEPBA nanocube	336 F g^{-1} (44.8 mAh g^{-1}) at 1 A g^{-1}	70.8 % after 3,000 cycles	3M KOH	This work
Cobalt PBA nanoparticle	250 F g^{-1} at 5 mV s^{-1}	93.5% after 5,000 cycles	0.5M Na_2SO_4	[3]
Mesoporous Cobalt PBA	295 F g^{-1} at 5 mV s^{-1}	50% after 100 cycles	1M $NaClO_4$	[4]
Ni-doped Cobalt PBA	466 F g^{-1} (129.4 mAh g^{-1}) at 5 mV s^{-1}	87.9% after 2,000 cycles	1M Na_2SO_4	[5]
CoFe PBA hollow nanocubes	2526 F g^{-1} at 0.5 A g^{-1}	90.25% after 2,000 cycles	3 M KOH	[6]
$K(MgMnFeNiCu)Fe(CN)_6$ HEPBA	175 F g^{-1} at 5 mV s^{-1}	-	1M Na_2SO_4	[7]
$K(MgMnCoNiCu)Fe(CN)_6$ HEPBA	160 F g^{-1} at 5 mV s^{-1}	-	1M Na_2SO_4	[7]
$K(MgMnFeCoNi)Fe(CN)_6$ HEPBA	135 F g^{-1} at 5 mV s^{-1}	-	1M Na_2SO_4	[7]

Table S6. OER EIS analysis.

Sample ID	Rs		Rct		CPE	
	Value (Ω)	error	Value (Ω)	error	Value (F)	error
CNM	0.49	0.003	9.32	0.058	0.87	0.003
CNMCu	0.91	0.006	4.26	0.032	0.83	0.006
CNMZn	0.83	0.004	7.83	0.055	0.79	0.003
CNMCuZn	0.81	0.005	3.07	0.029	0.82	0.007
CNM2CuZn	0.39	0.004	1.72	0.022	0.77	0.008
CNMCu2Zn	0.71	0.004	3.62	0.031	0.8	0.006
CNM2Cu2Zn	0.46	0.003	1.07	0.012	0.76	0.008

Table S7. Comparison of electrocatalytic performances of PBA-based materials.

Materials	**Overpotential**	**Stability**	**Refs**
NiFe PBA nanocube	258 mV at 10 mA cm^{-2}	100 h	[8]
FeCo PBA core shell	271 mV at 10 mA cm^{-2}	24 h	[9]
CoFe PBA nanocube	366 mV at 10 mA cm^{-2}	-	[10]
Co-Fe PBA nanocube	356 mV at 50 mA cm^{-2}	-	[11]
NiFe PBA hollow nanocube	389 mV at 20 mA cm^{-2}	-	[12]
CoFe-PBA/CFP nanosheet	314 mV at 10 mA cm^{-2}	-	[13]
CNM2CuZn HEPBA nanocube	242 mV at 10 mA cm^{-2} and 305 mV at 50 mA cm^{-2}	60 h	This work

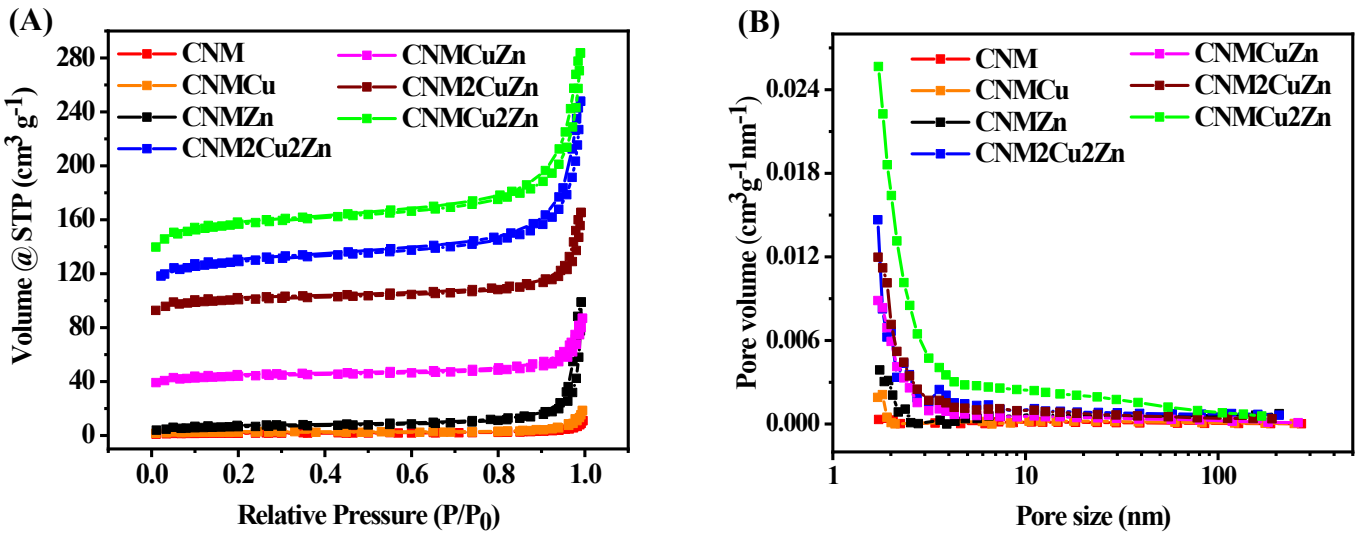

Figure S1. (A) Nitrogen gas adsorption and desorption isothermal. (B) Pore size distribution curves.

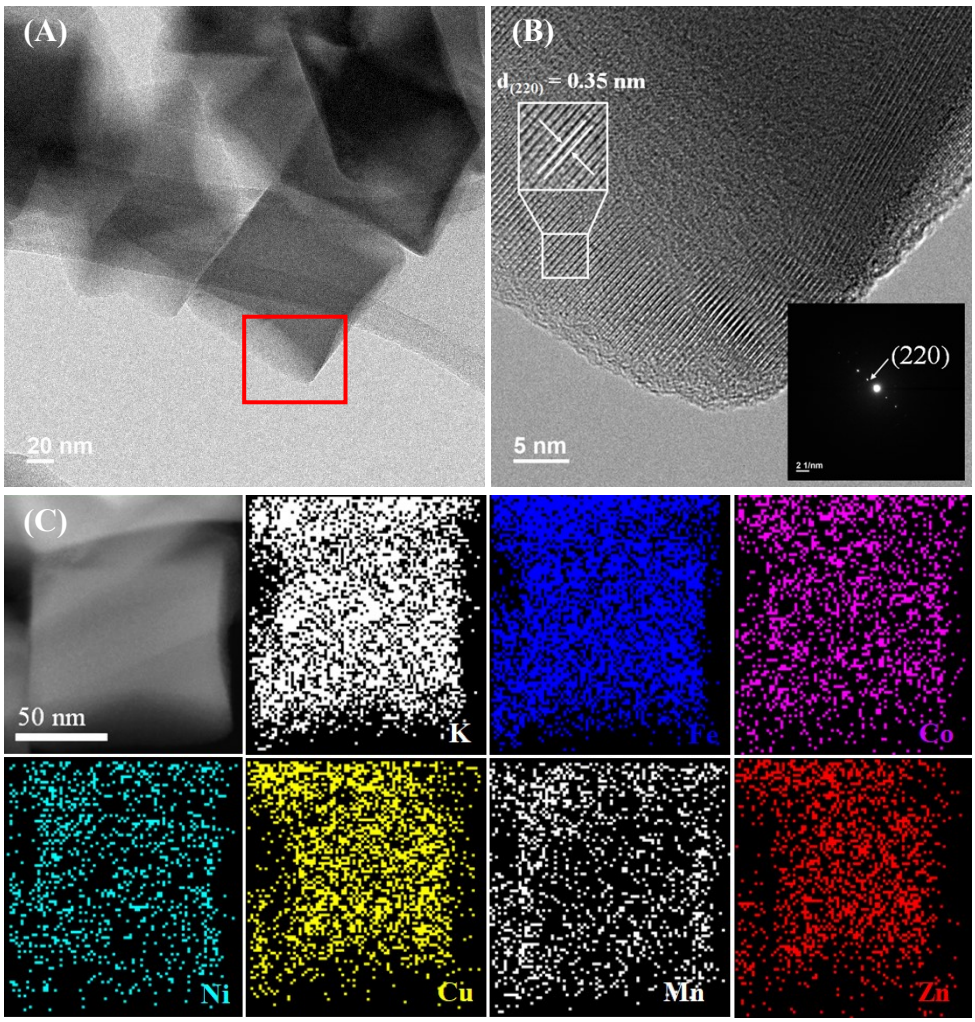

Figure S2. (A) TEM image, (B) HR-TEM image and NBED of red rectangle in (A), and (C) HAADF image and EDS mapping of CNM2CuZn.

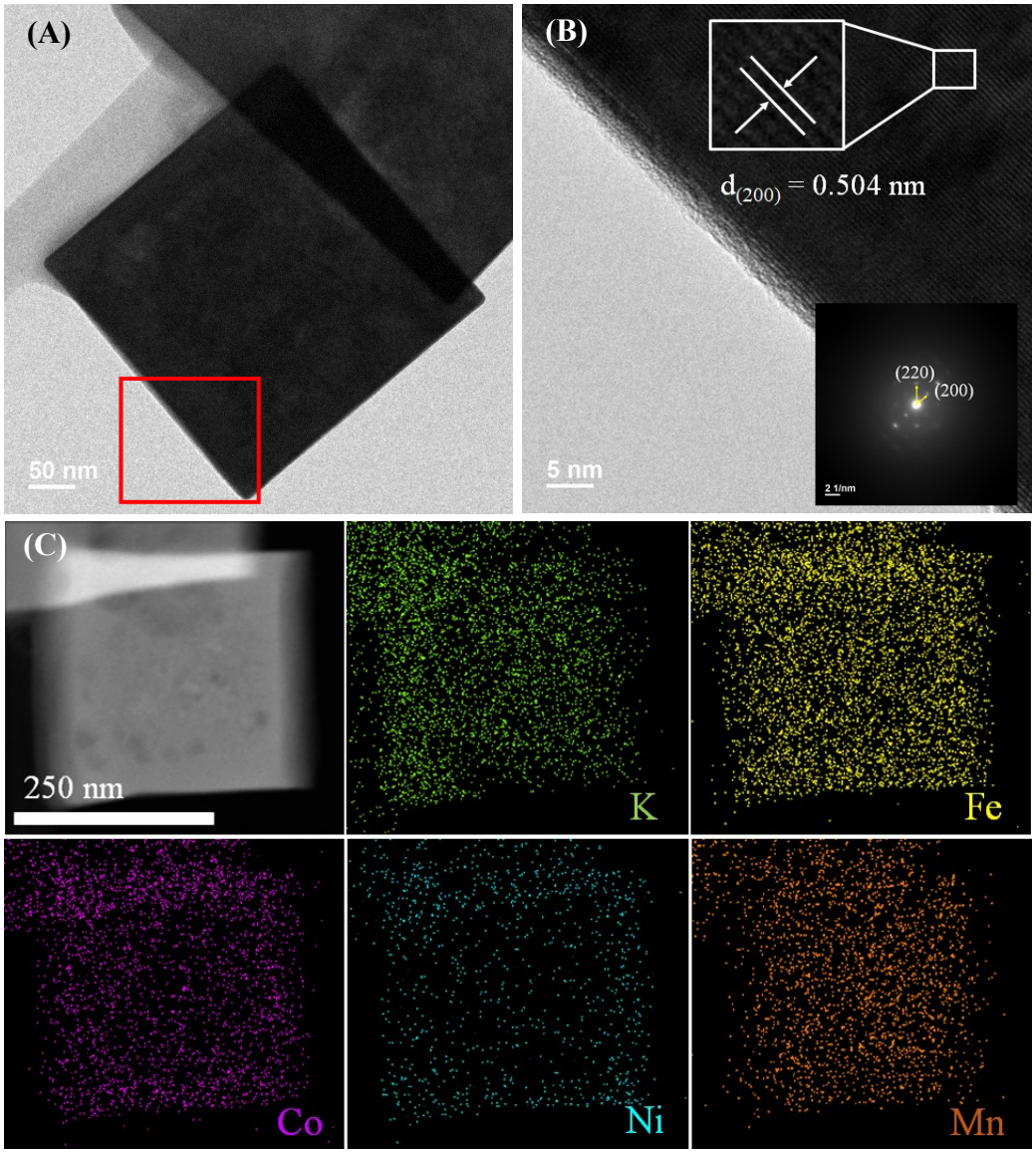

Figure S3. (A) TEM image, (B) HR-TEM image and NBED of red rectangle in (A), and (C) HAADF image and EDS mapping of CNM.

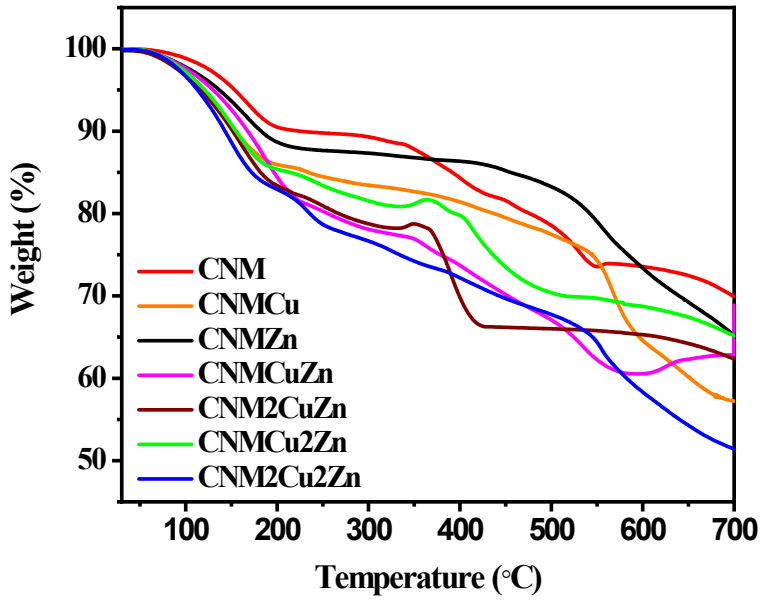

Figure S4. TGA analysis of various PBAs.

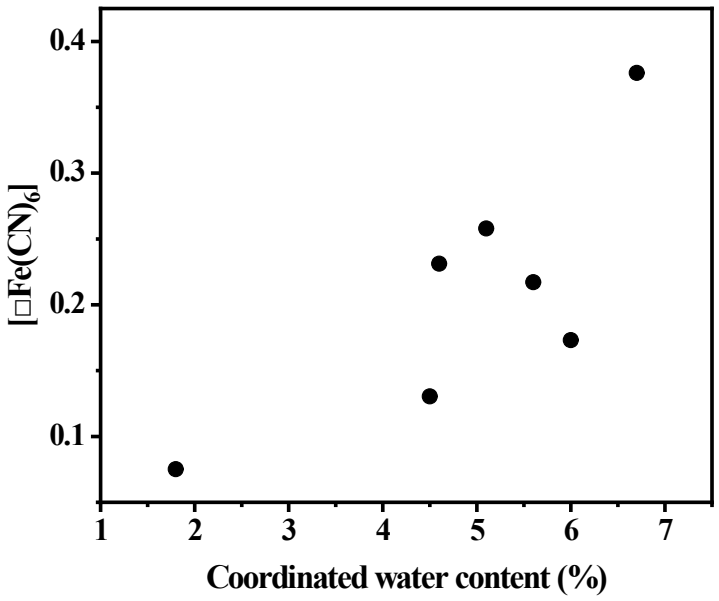

Figure S5. Relationship between coordinated water content and [□$Fe(CN)_6$].

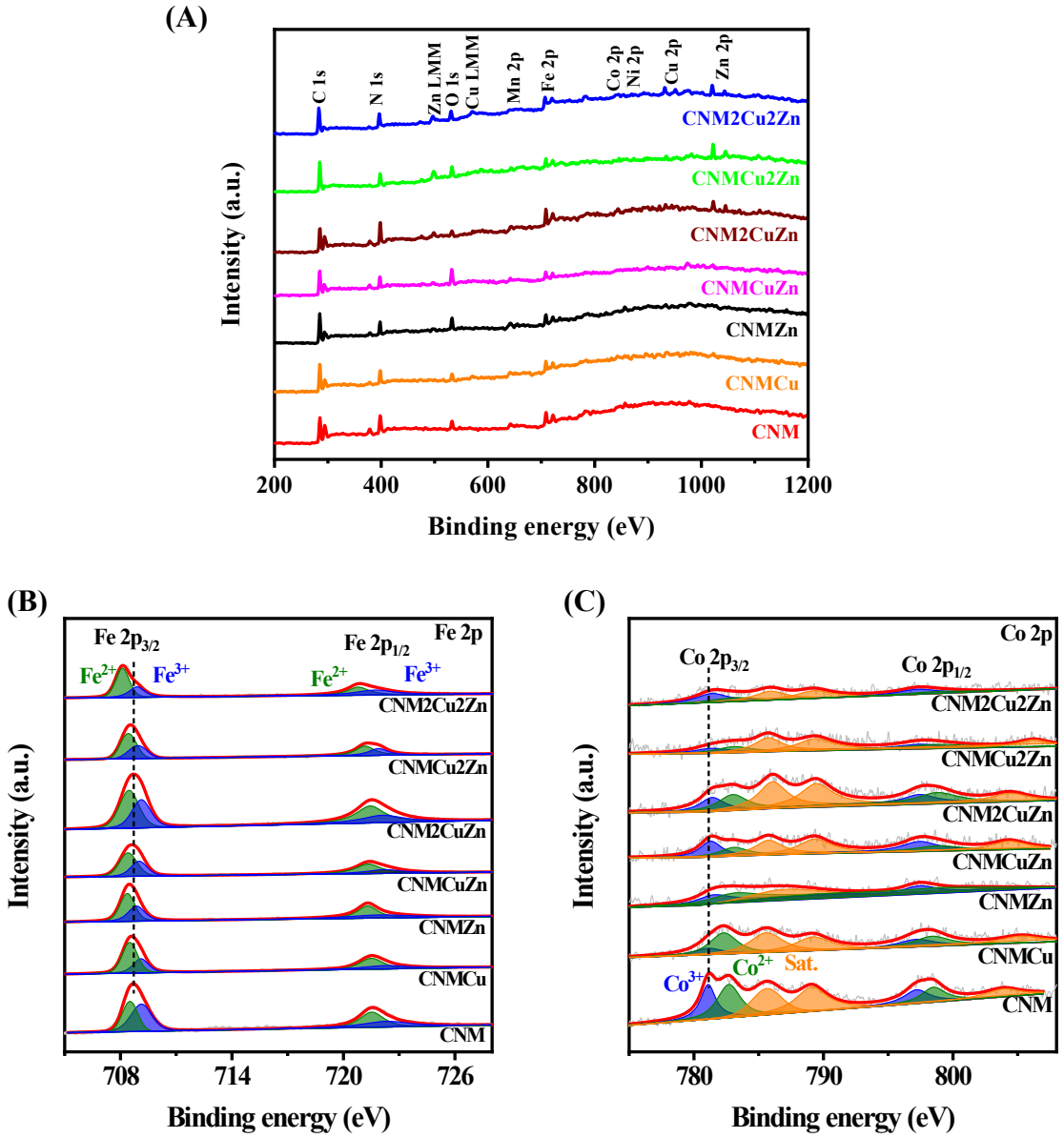
(A)
C 1s
N 1s
Zn LMM
O 1s
Cu LMM
Mn 2p
Fe 2p
Co 2p
Ni 2p
Cu 2p
Zn 2p
CNM2Cu2Zn
CNMCu2Zn
CNM2CuZn
CNMCuZn
CNMZn
CNMCu
CNM
Intensity (a.u.)
200
400
600
800
1000
1200
Binding energy (eV)
(B)
Fe 2p
Fe 2p3/2
Fe 2p1/2
Fe2+
Fe3+
Fe2+
Fe3+
CNM2Cu2Zn
CNMCu2Zn
CNM2CuZn
CNMCuZn
CNMZn
CNMCu
CNM
Intensity (a.u.)
708
714
720
726
Binding energy (eV)
(C)
Co 2p
Co 2p3/2
Co 2p1/2
CNM2Cu2Zn
CNMCu2Zn
CNM2CuZn
CNMCuZn
CNMZn
CNMCu
Co3+
Co2+
Sat.
CNM
Intensity (a.u.)
780
790
800
Binding energy (eV)

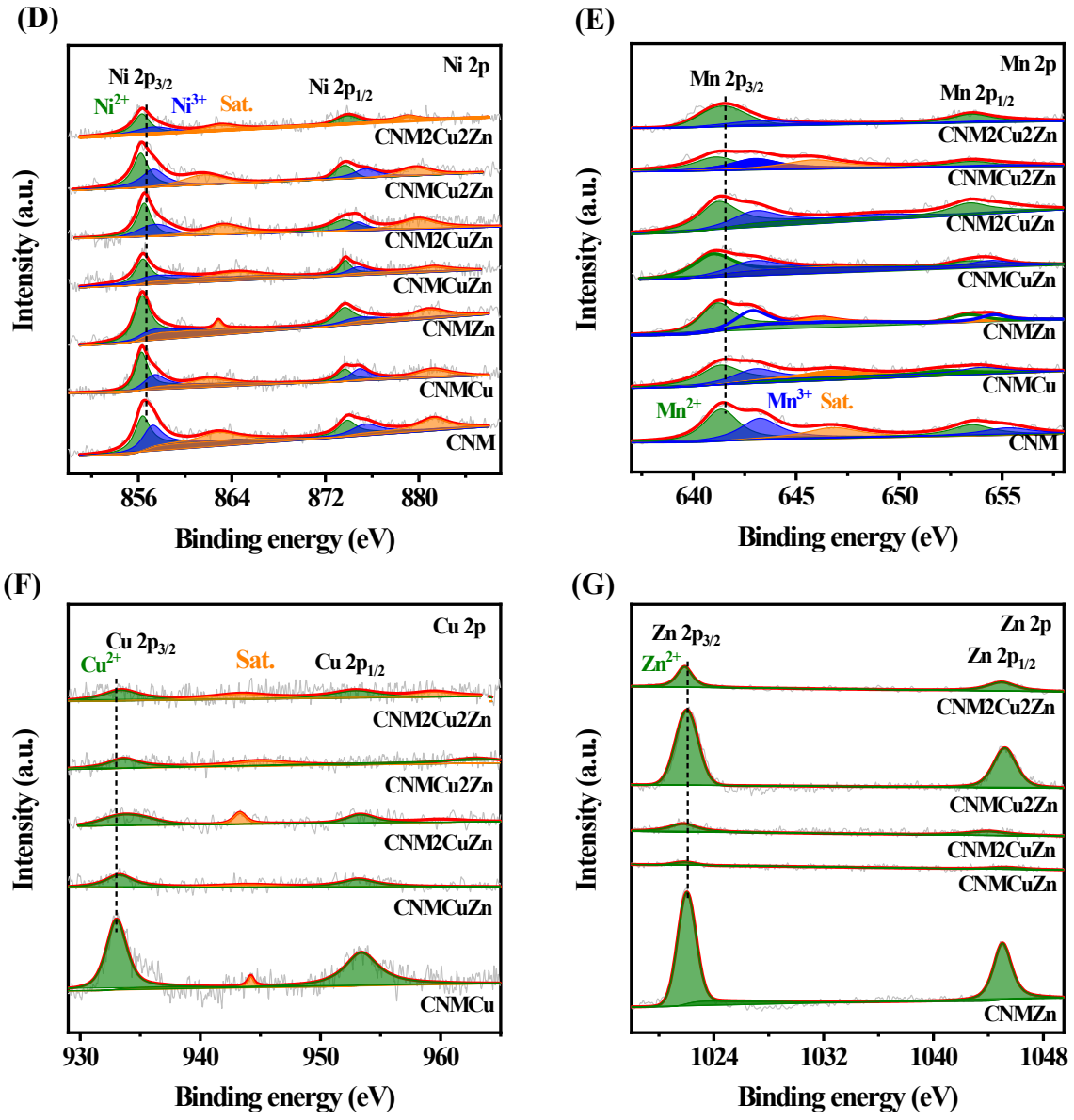

Figure S6. (A) XPS survey spectra of PBAs. High-resolution XPS spectra of PBAs. (B) Fe 2p, (C) Co 2p, (D) Ni 2p, (E) Mn 2p, (F) Cu 2p, and (G) Zn 2p.

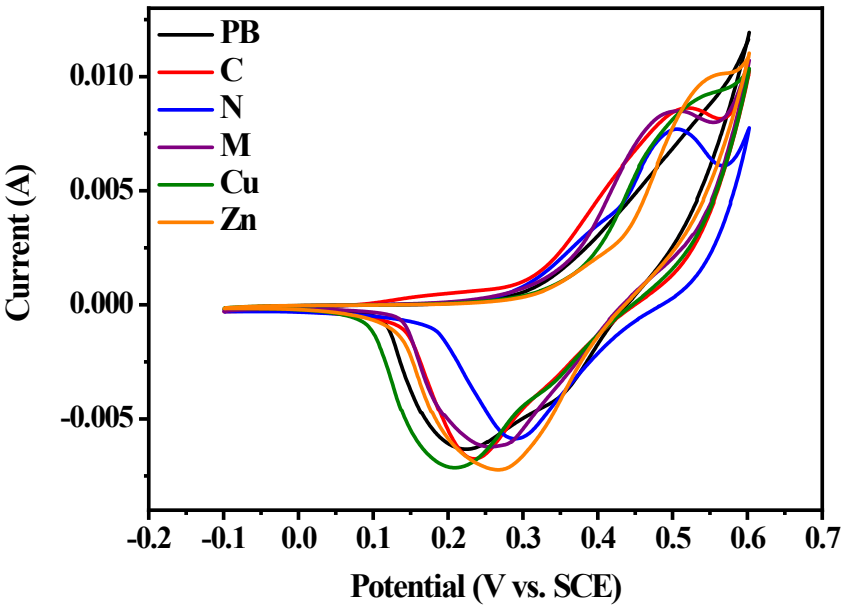

Figure S7. CV curve of the as-synthesized PB and unary-PBAs at a scan rate of 5 mV s^{-1}.

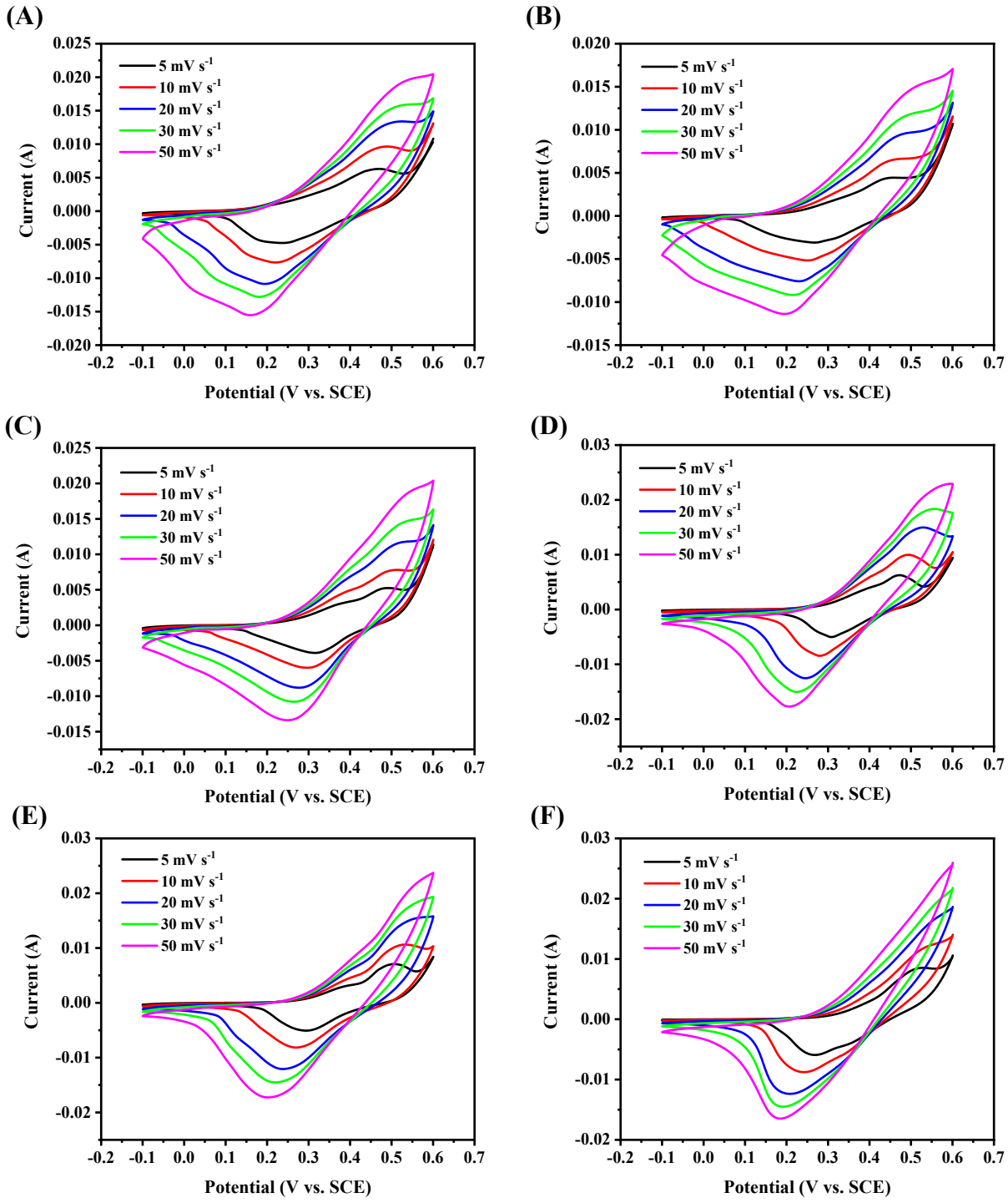
(A)
(B)
(C)
(D)
(E)
(F)
5 mV s-1
10 mV s-1
20 mV s-1
30 mV s-1
50 mV s-1
Current (A)
Potential (V vs. SCE)

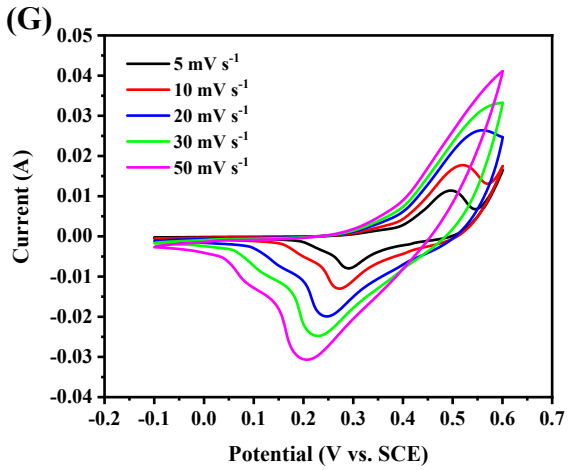

Figure S8. CV curves of various PBAs obtained at different scan rates from 5 to 50 mV s^{-1}. (A) CNM, (B) CNMCu, (C) CNMZn, (D) CNMCuZn, (E) CNM2CuZn, (F) CNMCu2Zn, and (G) CNM2Cu2Zn.

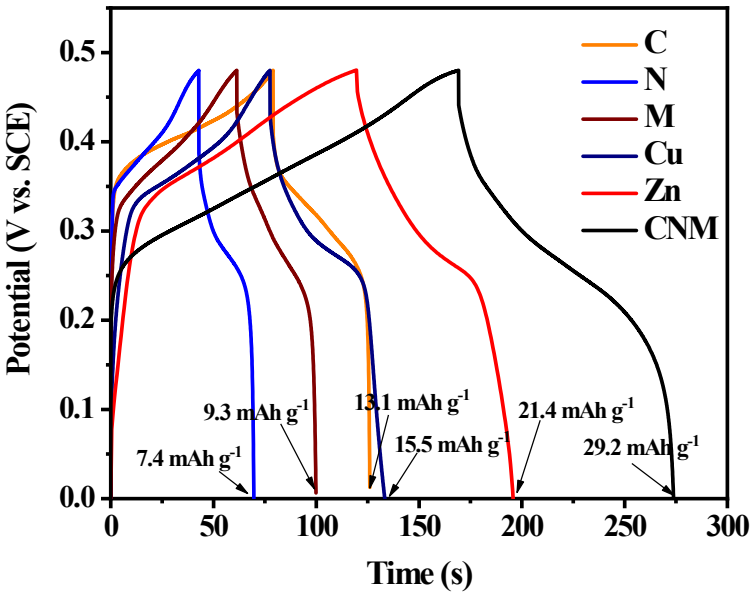

Figure S9. GCD curves of single-metal PBAs at a current density of 1 A g^{-1}.

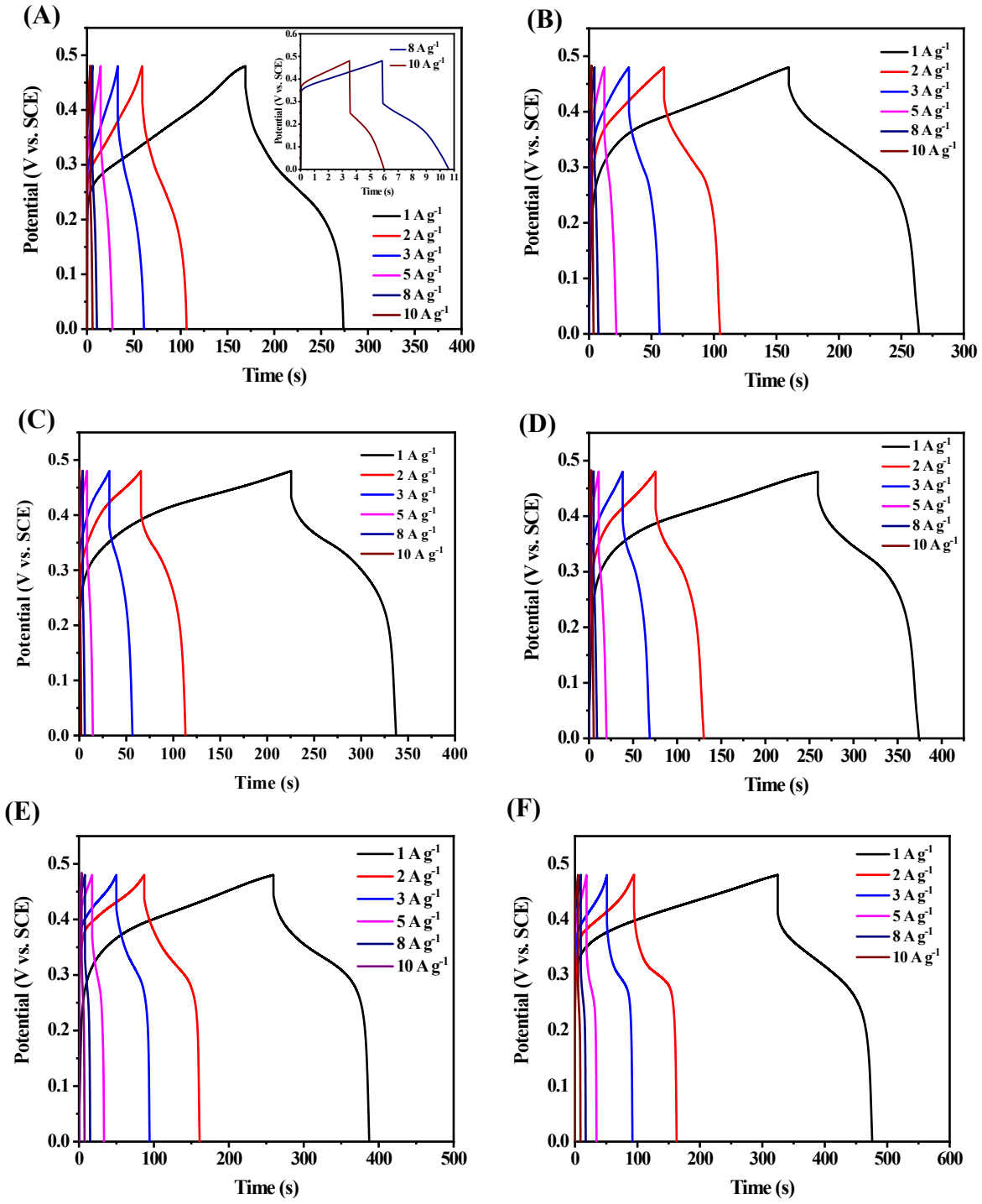
(A)
Potential (V vs. SCE)
Time (s)
1 A g-1
2 A g-1
3 A g-1
5 A g-1
8 A g-1
10 A g-1
(B)
Potential (V vs. SCE)
Time (s)
1 A g-1
2 A g-1
3 A g-1
5 A g-1
8 A g-1
10 A g-1
(C)
Potential (V vs. SCE)
Time (s)
1 A g-1
2 A g-1
3 A g-1
5 A g-1
8 A g-1
10 A g-1
(D)
Potential (V vs. SCE)
Time (s)
1 A g-1
2 A g-1
3 A g-1
5 A g-1
8 A g-1
10 A g-1
(E)
Potential (V vs. SCE)
Time (s)
1 A g-1
2 A g-1
3 A g-1
5 A g-1
8 A g-1
10 A g-1
(F)
Potential (V vs. SCE)
Time (s)
1 A g-1
2 A g-1
3 A g-1
5 A g-1
8 A g-1
10 A g-1

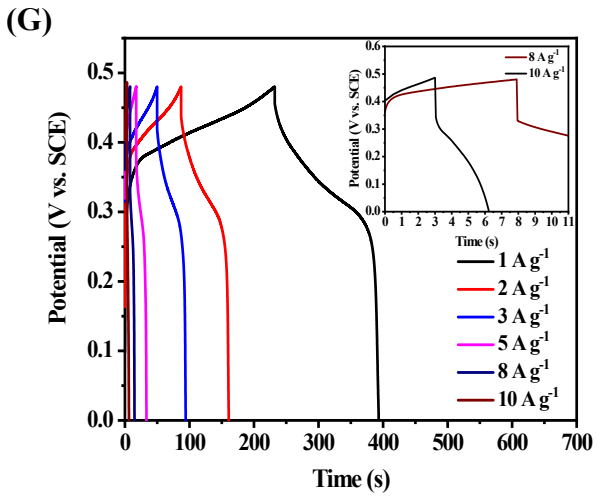

Figure S10. GCD curves of (A) CNM, (B) CNMCu, (C) CNMZn, (D) CNMCuZn, (E) CNM2CuZn, (F) CNMCu2Zn, and (G) CNM2Cu2Zn.

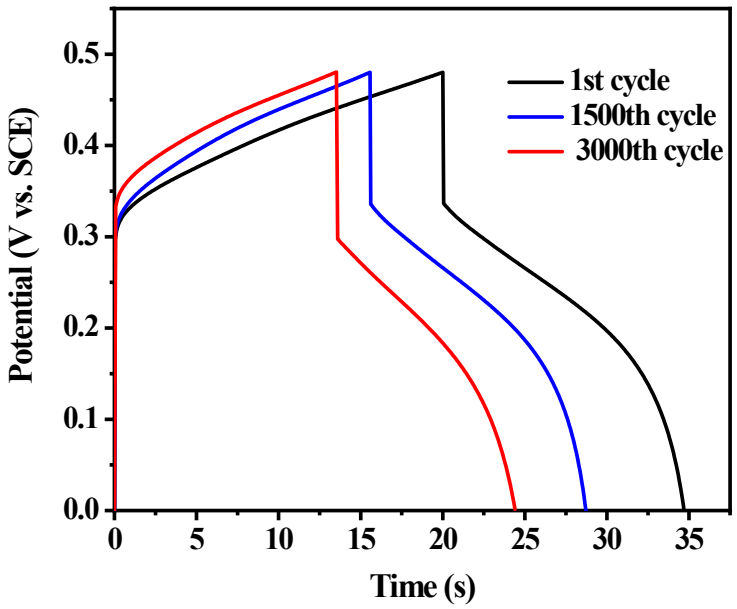

Figure S11. GCD curves of sample CNM2Cu2Zn at different stages during the cycle test.

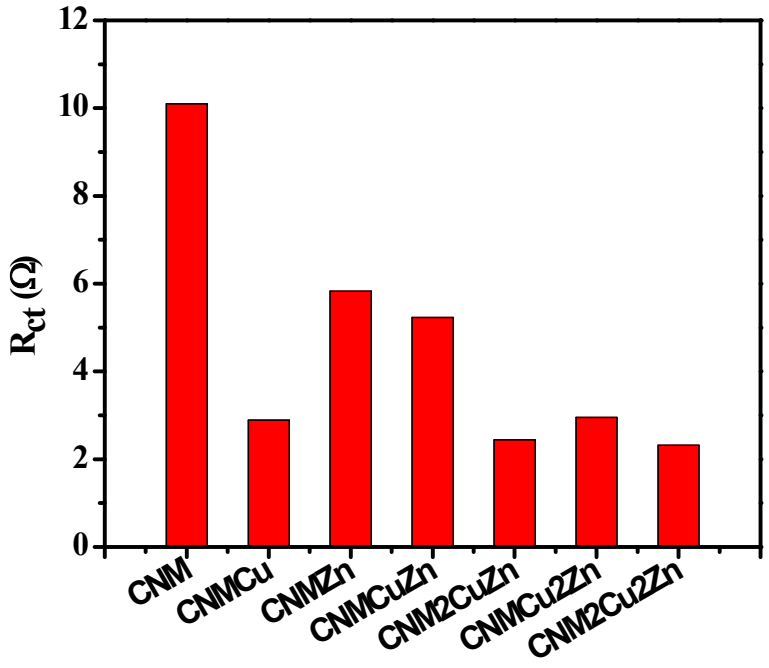

Figure S12. Charge transfer resistance of various PBAs.

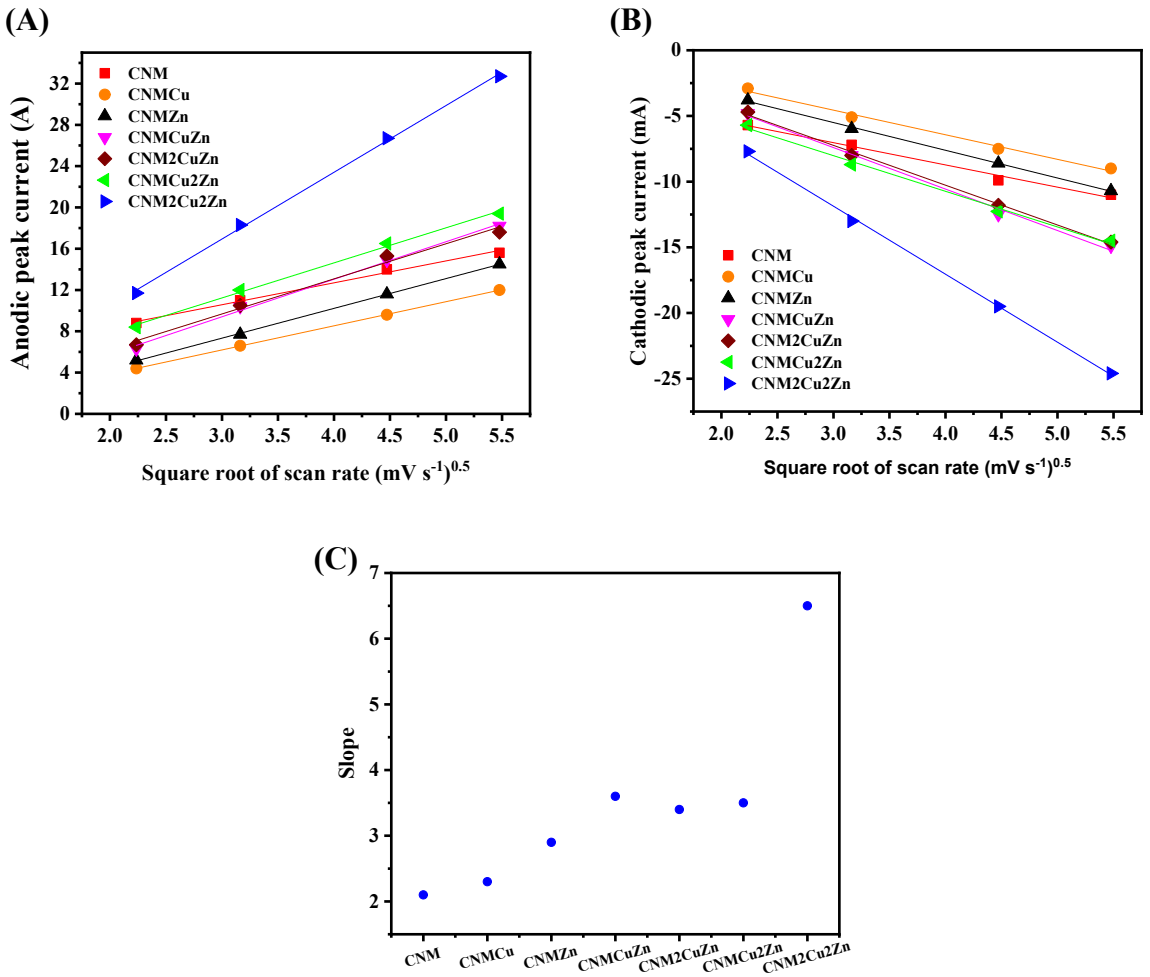

Figure S13. The peak current vs. square root of scan rate: (A) anodic and (B) cathodic. (C) Slopes, representing the ion diffusion coefficient, of various samples obtained from Figure (A).

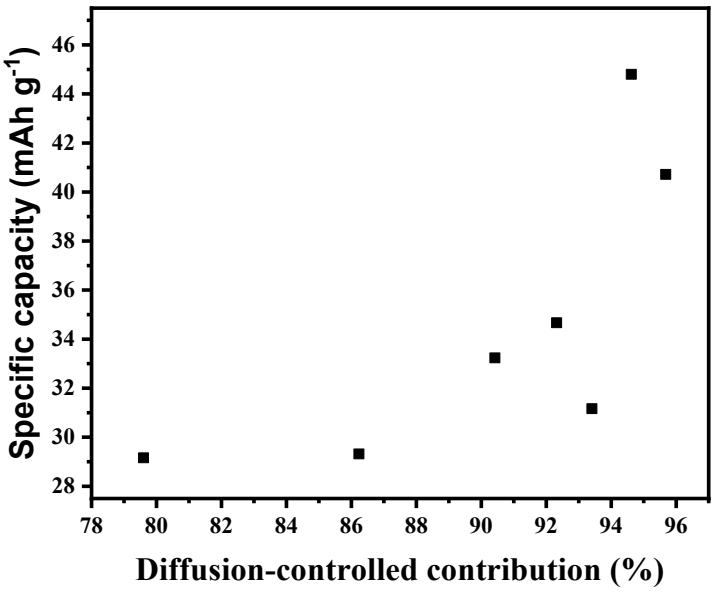

Figure S14. Specific capacity increases with the diffusion-controlled charge storage (calculated from CV curves at 5 mV s^{-1}).

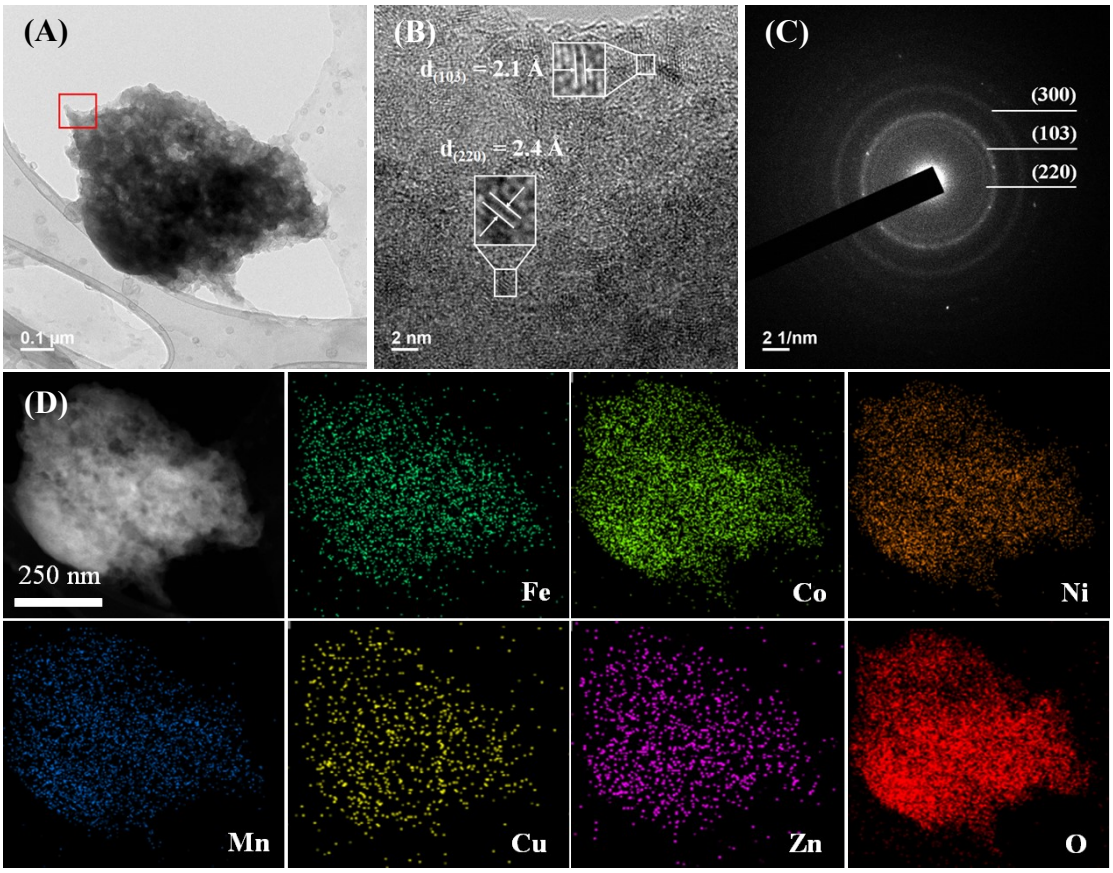

Figure S15. TEM of CNM2Cu2Zn after 10 cycles of charge-discharge. (A) TEM image, (B) HR-TEM image of red rectangle in (A), (C) SAED pattern of (B), and (D) HAADF image and EDS mapping.

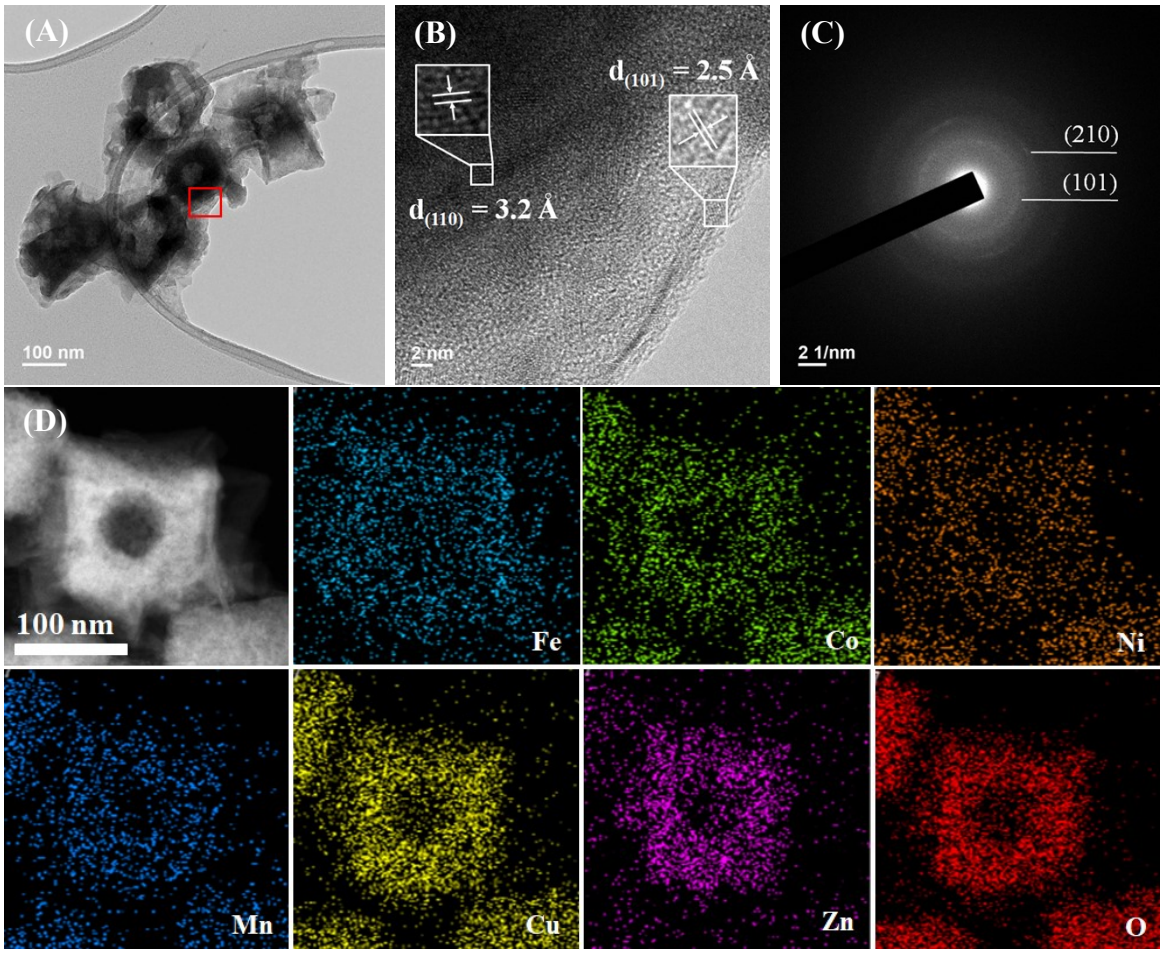

Figure S16. Post-TEM of CNM2CuZn after OER. (A) TEM image, (B) HR-TEM image of red rectangle in (A), (C) SAED pattern of (B), and (D) HAADF image and EDS mapping.

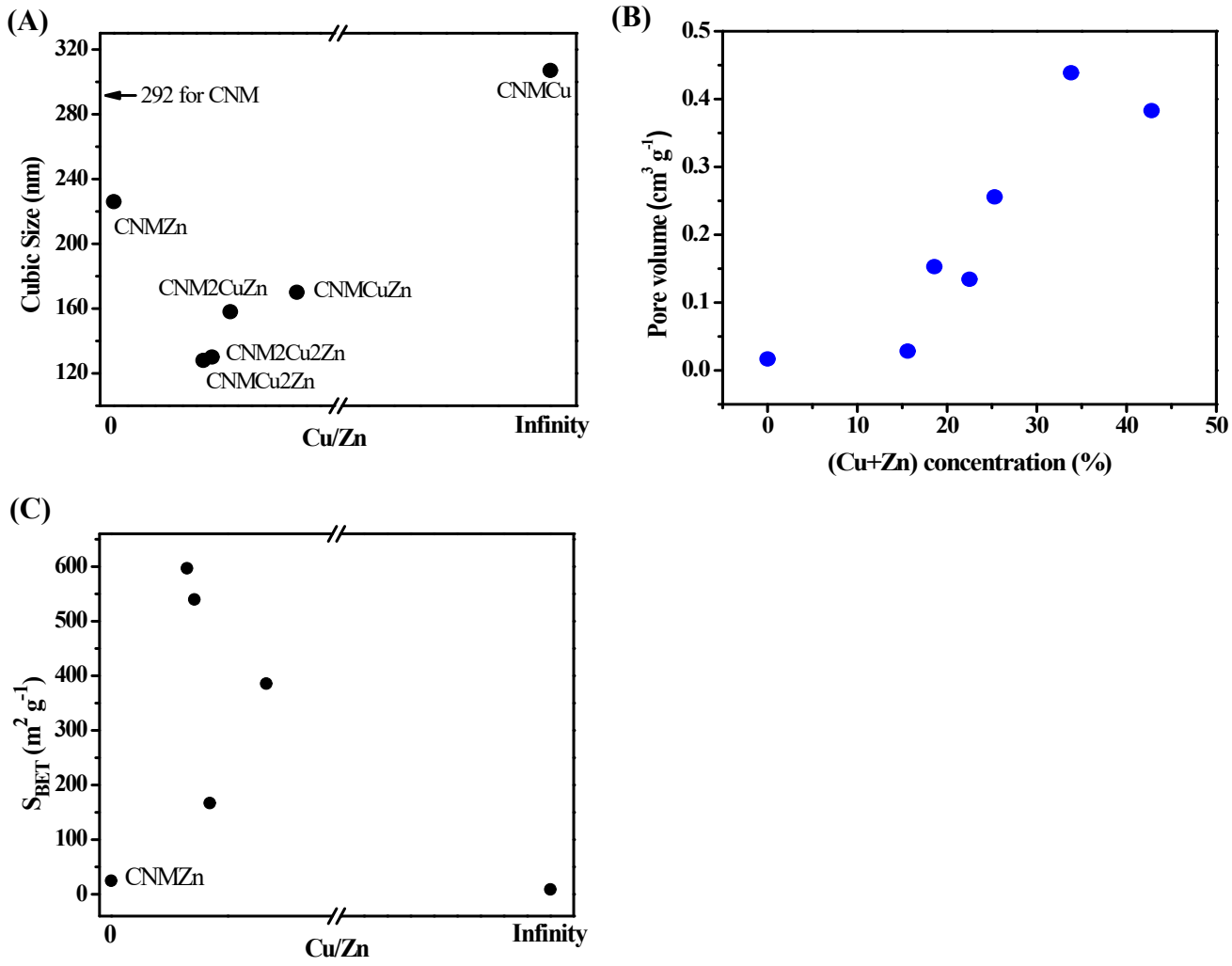

Figure S17. (A) Cubic size as a function of Cu/Zn ratio. (B) Pore volume increases with the (Cu+Zn) content. (C) BET surface area vs. Cu/Zn ratio.

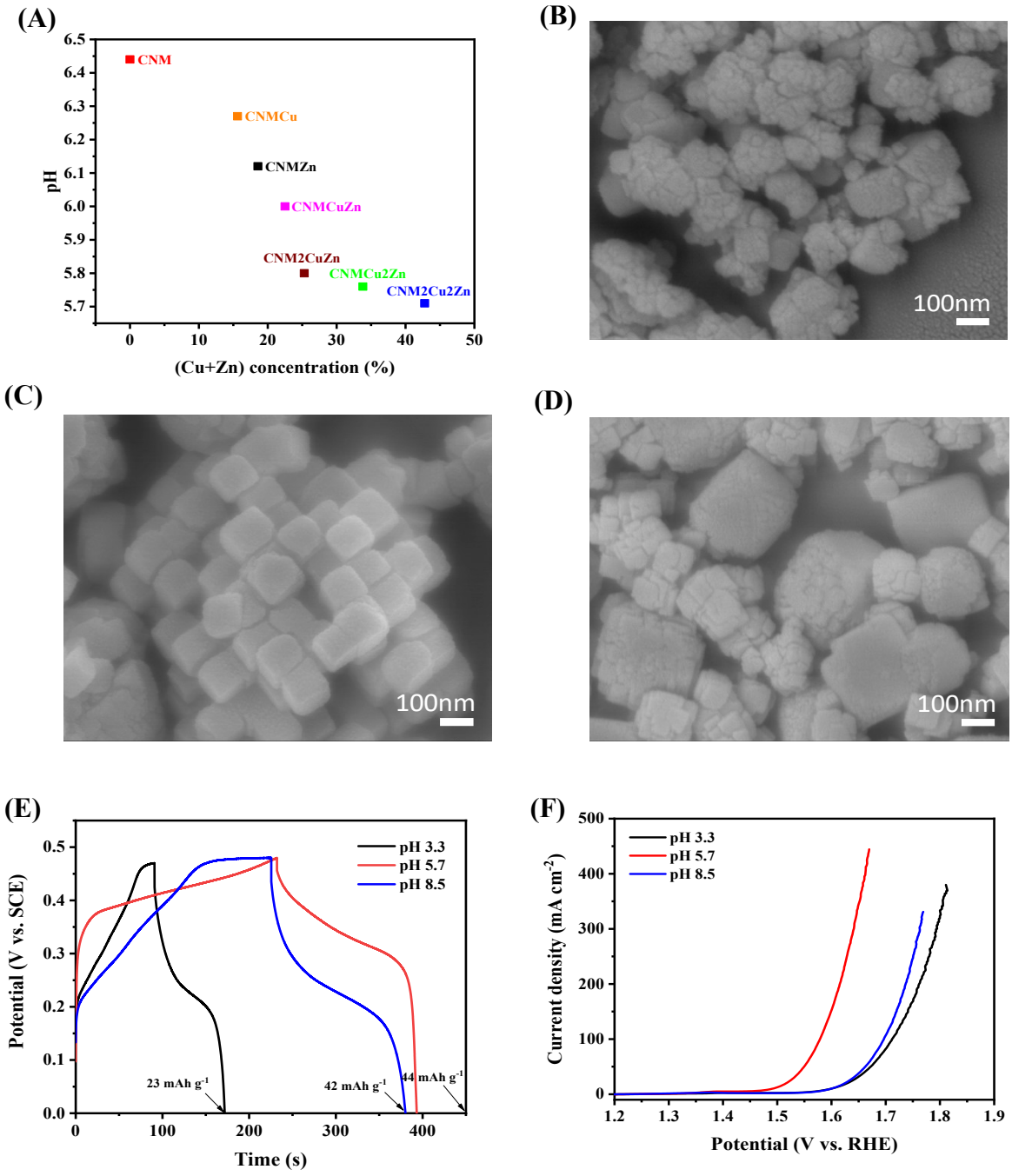

Figure S18. (A) pH value as function of the (Cu+Zn) concentration. SEM images of the CNM2Cu2Zn obtained at different precursor solution pH values: (B) 3.3, (C) 5.7, and (D) 8.5. (E) Capacity and (F) overpotential of CNM2Cu2Zn at different pH values.

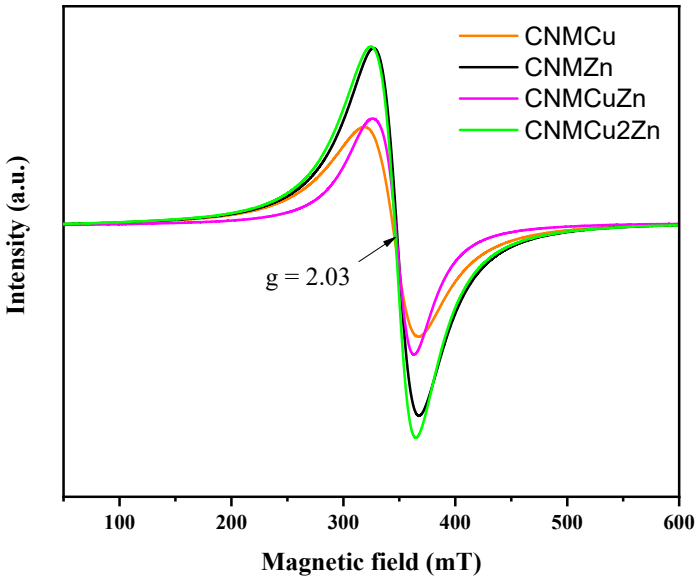

Figure S19. EPR analysis of various PBAs.

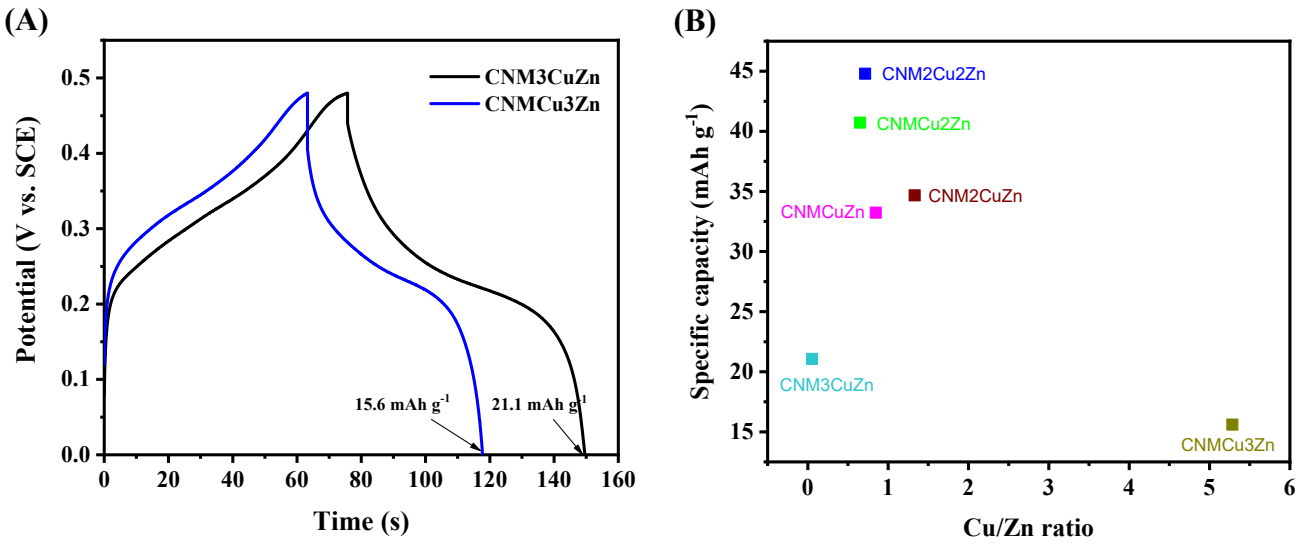

Figure S20. (A) GCD curves of CNM3CuZn and CNMCu3Zn at 1 A g^{-1}. (B) Cu/Zn ratio controls the specific capacity of HEPBAs.

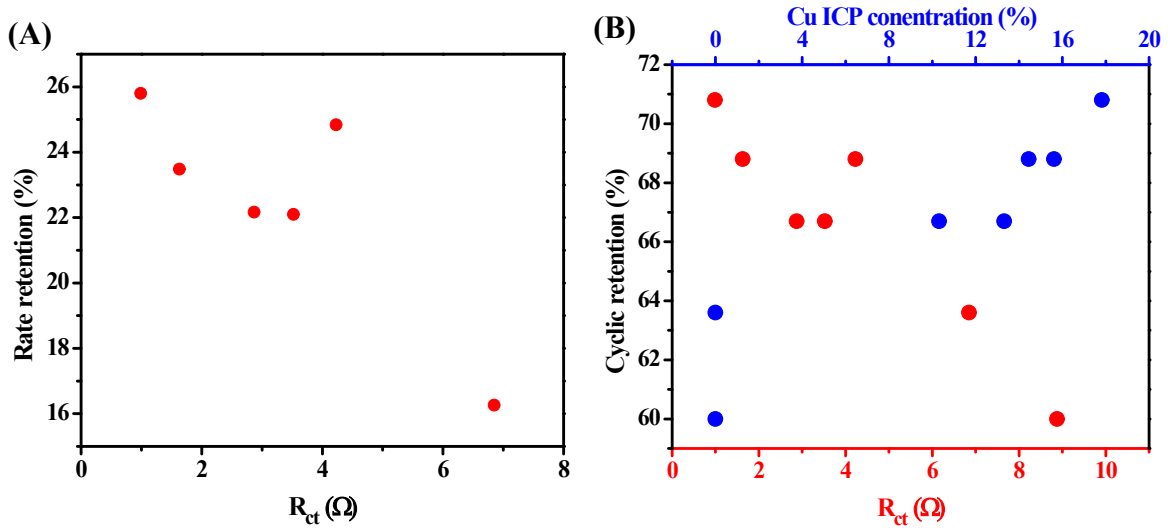

Figure S21. The effects of conductivity on the (A) rate retention and (B) cycle stability.

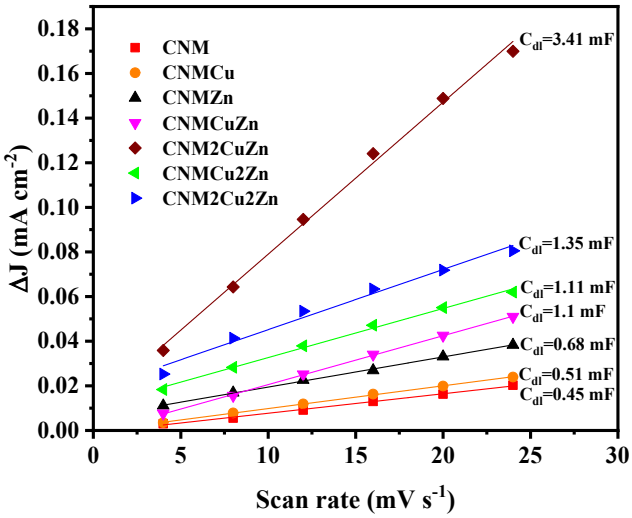

Figure S22. Cdl plots of PBAs.

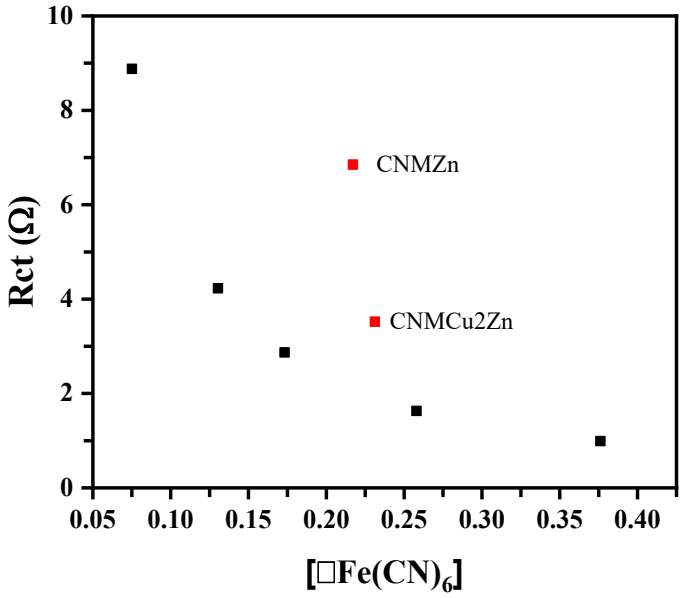

Figure S23. The correlation between the [□Fe(CN)$_6$] and Rct.

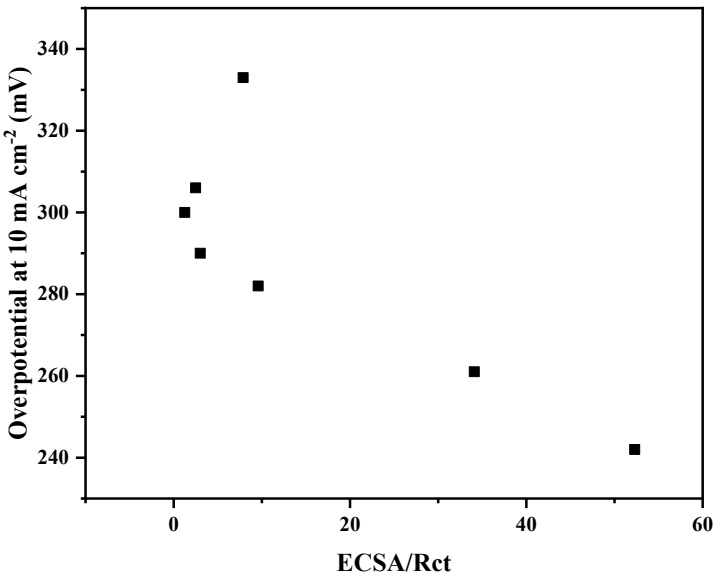

Figure S24. Overpotential decreases with ECSA/Rct.

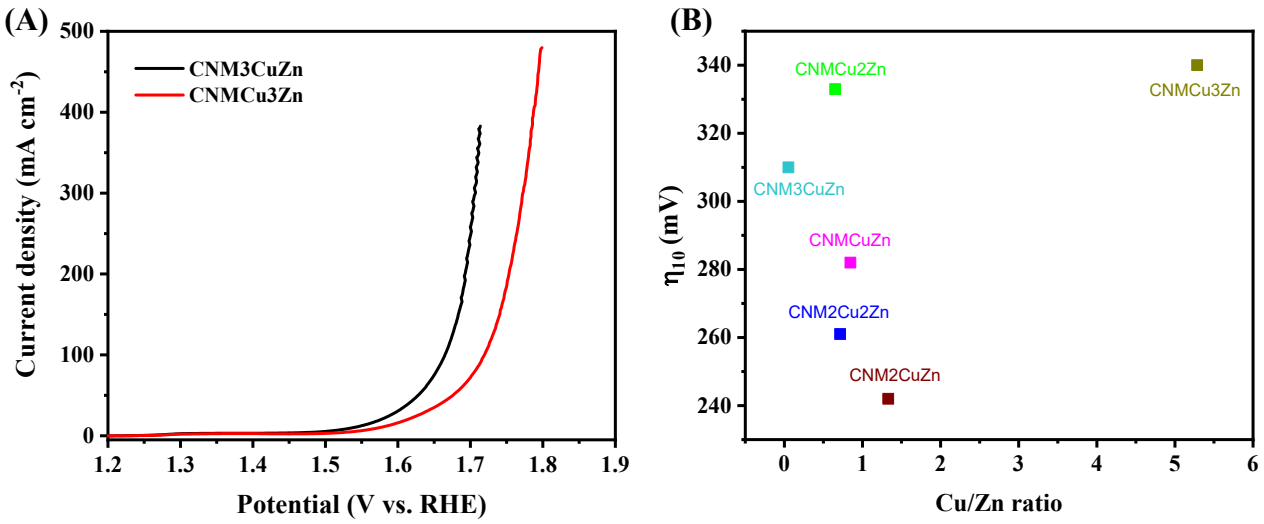

Figure S25. (A) LSV curves of CNM3CuZn and CNMCu3Zn at 1 A g^{-1}. (B) Cu/Zn ratio controls the overpotential of HEPBAs.

Reference

1. J.-W. Yeh, S.-K. Chen, S.-J. Lin, J.-Y. Gan, T.-S. Chin, T.-T. Shun, C.-H. Tsau and S.-Y. Chang, *Adv. Eng. Mater.*, 2004, **6**, 299-303.
2. Y. Ma, Y. Ma, Q. Wang, S. Schweidler, M. Botros, T. Fu, H. Hahn, T. Brezesinski and B. Breitung, *Energy Environ. Sci.*, 2021, **14**, 2883-2905.
3. F. Zhao, Y. Wang, X. Xu, Y. Liu, R. Song, G. Lu and Y. Li, *ACS Appl. Mater. Interfaces*, 2014, **6**, 11007-11012.
4. Y. Yue, Z. Zhang, A. J. Binder, J. Chen, X. Jin, S. H. Overbury and S. Dai, *ChemSusChem*, 2015, **8**, 177-183.
5. Y. Qiu, Y. Lin, H. Yang and L. Wang, *J. Alloys Comp.*, 2019, **806**, 1315-1322.
6. P. Zhu, X. Li, H. Yao and H. Pang, *J. Energy Storage*, 2020, **31**, 101544.
7. W. Jiang, T. Wang, H. Chen, X. Suo, J. Liang, W. Zhu, H. Li and S. Dai, *Nano Energy*, 2021, **79**, 105464.
8. X. Su, Y. Wang, J. Zhou, S. Gu, J. Li and S. Zhang, *J. Am. Chem. Soc.*, 2018, **140**, 11286-11292.
9. W. Zhang, H. Song, Y. Cheng, C. Liu, C. Wang, M. A. N. Khan, H. Zhang, J. Liu, C. Yu, L. Wang and J. Li, *Adv. Sci.*, 2019, **6**, 1801901.
10. H. Xu, H. Y. Shang, L. J. Jin, C. Y. Chen, C. Wang and Y. K. Du, *J Mater Chem A*, 2019, **7**, 26905-26910.
11. J. T. Hou, Z. M. Tang, K. Y. Wei, Q. X. Lai and Y. Y. Liang, *Catal Sci Technol*, 2021, **11**, 1110-1115.

12. M. M. Jiang, X. M. Fan, S. Cao, Z. H. Wang, Z. H. Yang and W. X. Zhang, *J Mater Chem A*, 2021, **9**, 12734-12745.

13. J. L. Wang, M. L. Zhang, J. H. Li, F. X. Jiao, Y. Lin and Y. Q. Gong, *Dalton T*, 2020, **49**, 14290-14296.